PHYSICAL REVIEW D **93,** 093012 (2016)

Atomic ionization by sterile-to-active neutrino conversion and constraints on dark matter sterile neutrinos with germanium detectors

Jiunn-Wei Chen,[1,2,3,*] Hsin-Chang Chi,[4] Shin-Ted Lin,[5,6] C.-P. Liu,[4,†] Lakhwinder Singh,[5,7] Henry T. Wong,[5] Chih-Liang Wu,[1,5,3] and Chih-Pan Wu[1,5,‡]

[1]*Department of Physics and Center for Theoretical Sciences, National Taiwan University, Taipei 10617, Taiwan*
[2]*Leung Center for Cosmology and Particle Astrophysics, National Taiwan University, Taipei 10617, Taiwan*
[3]*Center for Theoretical Physics, Massachusetts Institute of Technology, Cambridge, Massachusetts 02139, USA*
[4]*Department of Physics, National Dong Hwa University, Shoufeng, Hualien 97401, Taiwan*
[5]*Institute of Physics, Academia Sinica, Taipei 11529, Taiwan*
[6]*College of Physical Science and Technology, Sichuan University, Chengdu 610064, China*
[7]*Department of Physics, Banaras Hindu University, Varanasi 221005, India*

(Received 27 January 2016; published 19 May 2016)

The transition magnetic moment of a sterile neutrino can give rise to its conversion to an active neutrino through radiative decay or nonstandard interaction (NSI) with matter. For sterile neutrinos of keV-mass as dark matter candidates, their decay signals are actively searched for in cosmic x-ray spectra. In this work, we consider the NSI that leads to atomic ionization, which can be detected by direct dark matter experiments. It is found that this inelastic scattering process for a nonrelativistic sterile neutrino has a pronounced enhancement in the differential cross section at energy transfer about half of its mass, manifesting experimentally as peaks in the measurable energy spectra. The enhancement effects gradually smear out as the sterile neutrino becomes relativistic. Using data taken with low-threshold low-background germanium detectors, constraints on sterile neutrino mass and its transition magnetic moment are derived and compared with those from astrophysical observations.

DOI: 10.1103/PhysRevD.93.093012

I. INTRODUCTION

Sterile neutrinos are of interest in particle physics, astrophysics, and cosmology. In addition to the three known "active" neutrinos, they are invoked in many beyond-Standard-Model theories to address fundamental questions such as explaining the origin of neutrino masses (for instance, via various types of seesaw mechanisms), providing suitable dark matter candidates (for their being massive and noninteracting with matter), and setting the stage of leptogenesis that subsequently leads to the baryon asymmetry of the universe.

As sterile neutrinos are singlets in the Standard Model gauge groups, their masses, mixing angles, and couplings are unknown *a priori*. Different models have their own preferred parameter spaces by construction, and can only be constrained by experiments. The type I seesaw mechanism [1–5] provides a nice explanation for the smallness of active neutrino masses, but the predicted sterile neutrino masses at the grand unified theory scale make their experimental confirmation extremely difficult. On the other hand, there are other low-energy seesaw mechanisms that predict the existence of light sterile neutrinos (for a recent, comprehensive overview, see the community white paper [6]). Two particularly interesting cases have their lightest sterile neutrino masses to be (i) eV scale (see, e.g., Refs. [7,8]), which is motivated by the LSND [9] and reactor [10] anomalies etc., and (ii) keV scale (see, e.g., Refs. [11,12]), which can be a good dark matter candidate [13–16].[1] In this work, we shall focus on the latter case.

Massive sterile neutrinos can undergo radiative decays via their mixing with the active SM light neutrinos. This process is considered as one of the golden modes to look for keV-scale sterile neutrinos. Anomalies in the measurements of x-ray spectra from astrophysical objects such as galaxies or galaxies clusters [17,18] may be signatures of sterile neutrinos. Recently there are two groups reporting abnormal x-ray emission lines—one at $E = (3.55 - 3.57) \pm 0.03$ keV in a stacked XMM-Newton spectrum of 73 galaxy clusters [19], and the other at $E = 3.52 \pm 0.02$ keV in spectra of the Andromeda galaxy and the Perseus galaxy cluster [20]. These two papers triggered a huge amount of theoretical interpretations, and the possibility of a decaying sterile neutrino with mass

*jwc@phys.ntu.edu.tw
†cpliu@mail.ndhu.edu.tw
‡jpw750811@gmail.com

[1]We adopt the natural units $\hbar = c = 1$ in this paper, so mass and energy have the same dimension.

$m_s = 7.1$ keV and its mixing to active neutrino mixing with an angle $\sin^2(2\theta) \sim (5\text{–}7) \times 10^{-11}$ was suggested [19,20].

Motivated by this anomalous x-ray emission line and its possible interpretation of radiative sterile neutrino decay, we consider in this paper an effective Lagrangian that gives rise to the coupling of an incoming sterile neutrino, an outgoing active neutrino, and a virtual photon (see the left panel of Fig. 1). When the virtual photon couples to electromagnetic currents of normal matter, this will generate some nonstandard interaction between the sterile neutrino and normal matter, and the signals in forms of normal matter recoils can be searched for with typical direct dark matter detectors (see the right panel of Fig. 1). Such direct detection experiments can provide complementary constraints on sterile neutrino properties to the above indirect astrophysical searches in x-ray spectra, which originate from the same effective Lagrangian with the photon becomes real, outgoing, thus observable.

The specific process we study is atomic ionization of matter during the conversion of sterile to active neutrinos via their transition magnetic moments. One interesting feature of this process is the exchanged photon can go across the spacelike region (typical for t-channel processes) to the timelike region (e.g., the final active, massless neutrino has almost zero four momentum so the square of 4-momentum transfer is simply $\sim m_s^2$), because the two-body atomic final state (an ion plus an ionized electron) can make this kinematically possible. As a result, there is a big enhancement from the real photon pole in the cross section.

For nonrelativistic (NR) sterile neutrinos with keV-mass, low-energy detectors with capability of sub-keV thresholds are required. For this reason we focus on germanium detectors and use their data to set constraints on sterile neutrino properties. We also note that there are related studies, for example, the active-to-sterile neutrino conversion in magnetic environments of the early universe [21] and supernovae [22]; sterile neutrino production by the Primakoff effect in neutrino beams [23]; and implications of sterile neutrinos in searches of magnetic moments of active neutrinos [24].

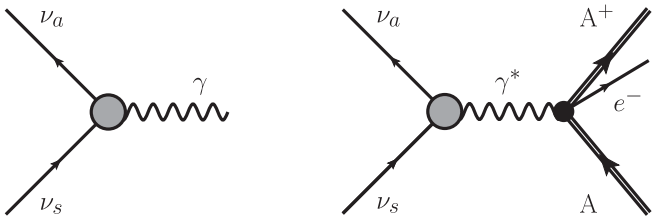

FIG. 1. Left: The radiative decay of a sterile neutrino to an active neutrino where the shaded circle represents its transition magnetic moment. Right: The atomic ionization induced by the transition magnetic moment of a sterile neutrino where the intermediate photon is virtual.

The paper is organized as follows. In Sec. II, we introduce the basic formalism that describes the atomic ionization caused by the transition magnetic moment of a sterile neutrino, and emphasize the differences from the more familiar cases where incoming and outgoing neutrinos are nearly mass degenerate. In Secs. III and IV, we present and discuss our results for hydrogen and germanium ionization, respectively. Using data taken by germanium detectors, we derive the bounds on sterile neutrino properties in Sec. V, and conclude in Sec. VI.

II. FORMALISM

The radiative decay of a sterile neutrino ν_s into a Standard-Model neutrino ν_a, $\nu_s \to \nu_a + \gamma$, can be effectively formulated by the interaction Lagrangian,

$$\mathcal{L}_{\nu_s\nu_a\gamma} = \frac{\mu_{\nu_{sa}} e}{2m_e} \frac{1}{2} \bar{\nu}_a \sigma_{\mu\nu} \nu_s F^{\mu\nu}, \tag{1}$$

where $\sigma_{\mu\nu} = \frac{i}{2}[\gamma_\mu, \gamma_\nu]$ is the tensor Dirac matrix and $F^{\mu\nu} = \partial^\mu A^\nu - \partial^\nu A^\mu$ is the field strength of the photon field A^μ. The coupling constant $\mu_{\nu_{sa}}$ can be understood as the transition magnetic moment measured in units of Bohr's magneton, $e/(2m_e)$, that induces a ν_s–ν_a transition. In the limit that ν_a is massless, the total decay width is

$$\Gamma_{\nu_s \to \nu_a \gamma} = \left(\frac{\mu_{\nu_{sa}} e}{2m_e}\right)^2 \frac{m_s^3}{8\pi}. \tag{2}$$

In case ν_s oscillates into ν_a by a mixing angle θ, the transition magnetic moment can arise from one-loop radiative corrections. As calculated in [25],

$$\mu_{\nu_{sa}} = \frac{3G_F}{4\sqrt{2}\pi^2} m_e m_s \sin\theta, \tag{3}$$

where G_F is the Fermi constant. This leads to the familiar expression that relates $\Gamma_{\nu_s \to \nu_a \gamma}$ to the oscillation angle of sterile neutrinos,

$$\Gamma^{(\mathrm{osc})}_{\nu_s \to \nu_a \gamma} = \frac{9}{1024\pi^4} G_F^2 \alpha \sin^2(2\theta) m_s^5, \tag{4}$$

where $\alpha = e^2/(4\pi)$ is the fine structure constant.

With $\mathcal{L}_{\nu_s\nu_a\gamma}$, it is also possible to consider processes in which a ν_s is converted to a ν_a by scattering off an electromagnetic source and the exchanged photon is virtual. In this article, we are interested in atomic ionization, i.e.,

$$\nu_s + \mathrm{A} \to \nu_a + \mathrm{A}^+ + e^-,$$

because the recoiled electron can be detected as a signal of such a ν_s–ν_e conversion. This process resembles the one involving only SM neutrinos,

$$\nu_a + \mathrm{A} \to \nu_{a'} + \mathrm{A}^+ + e^-,$$

except for different mass and kinematics of the incident neutrinos. We shall not repeat a full derivation of the scattering formalism for this sterile neutrino case, but only present the main cross section formulas and highlight its differences from the SM neutrino case (whose details can be found in [26]).

The single differential cross section with respect to the energy transfer T by neutrinos is expressed in the form

$$\frac{d\sigma}{dT} = \int d\cos\theta \frac{2\pi\alpha^2}{(q^2)^2}\frac{|\vec{k}_a|}{|\vec{k}_s|}\left(\frac{\mu_{\nu_{\mathrm{sa}}}}{2m_e}\right)^2 (V_L R_L + V_T R_T), \quad (5)$$

where $\vec{k}_s$ and $\vec{k}_a$ are the 3-momenta of the incoming and outgoing neutrinos, respectively; $q^2 = q_\mu q^\mu$ is the square of the 4-momentum transfer $q_\mu = (T, \vec{q})$; and the integration over the scattering angle of neutrino, θ, is confined in the range

$$\min\left\{1, \max\left[-1, \frac{\vec{k}_s^2 + \vec{k}_a^2 - 2M(T-B)}{2|\vec{k}_s||\vec{k}_a|}\right]\right\} \le \cos\theta \le 1, \quad (6)$$

with $M = m_{\mathrm{A}^+} + m_e$ being the total mass of the final $\mathrm{A}^+ + e^-$ system and B the binding energy of the ejected electron.

The unpolarized longitudinal and transverse response functions, R_L and R_T, which are functions of T and $|\vec{q}|$, are defined by

$$R_L = \sum_f \overline{\sum_i} |\langle f|\rho^{(A)}(\vec{q})|i\rangle|^2 \delta\left(T - B - \frac{\vec{q}^2}{2M} - \frac{\vec{p}_r^2}{2\mu}\right), \quad (7)$$

$$R_T = \sum_f \overline{\sum_i} |\langle f|\vec{j}_\perp^{(A)}(\vec{q})|i\rangle|^2 \delta\left(T - B - \frac{\vec{q}^2}{2M} - \frac{\vec{p}_r^2}{2\mu}\right). \quad (8)$$

The former depends on the atomic charge density $\rho^{(A)}(\vec{q})$ and the latter on the atomic transverse (perpendicular to $\vec{q}$) current density $\vec{j}_\perp^{(A)}(\vec{q})$. For all processes we are going to discuss in this paper, the nuclear charge and current densities are negligible. Note that the spin states of the initial atom $|i\rangle$ are averaged (hence the symbol $\overline{\sum}_i$) and the final states $|f\rangle$ are summed (integrated if quantum numbers are continuous). The delta function imposes the condition of energy conservation, and the total energy of the final $\mathrm{A}^+ + e^-$ system is separated into the center-of-mass part $\vec{q}^2/(2M)$ and the internal part $\vec{p}_r^2/(2\mu)$, where $\vec{p}_r$ is the relative momentum and the reduced mass $\mu = m_e m_{\mathrm{A}^+}/M \approx m_e$.

Because the incoming and outgoing neutrinos have different masses, the kinematic factors V_L and V_T now become

$$V_L = \frac{-q^4}{|\vec{q}|^4}((m_s+m_a)^2|\vec{q}|^2 + (E_s+E_a)^2 q^2 + (m_s^2-m_a^2)^2 - 2(E_s^2-E_a^2)(m_s^2-m_a^2)), \quad (9)$$

$$V_T = -\left((m_s+m_a)^2 - \frac{(m_s^2-m_a^2)^2}{q^2}\right)q^2 - \frac{q^2(4|k_s|^2|k_a|^2 - (|k_s|^2+|k_a|^2-|\vec{q}|^2)^2)}{2|\vec{q}|^2}. \quad (10)$$

If one sets $m_s = m_a = m_l$, then the above results converge to Eqs. (13) and (14) of Ref. [26]. Because of the square of the photon propagator, the V_T/q^4 term in Eq. (5) has a double pole in q^2 with the coefficient $(m_s^2 - m_a^2)^2$ and the remaining part has a single pole in q^2. On the contrary, the V_L/q^4 term does not contain any pole in q^2. In cases where $q^2 = 0$ is never reached, for example, elastic scattering, $\nu_s + \mathrm{A} \to \nu_a + \mathrm{A}$, where $q^2 = -2M_{\mathrm{A}}T$, there is no singularity in $d\sigma/dT$. However, the situation is quite different when the atom is ionized into a two-body system $\mathrm{A}^+ + e^-$. For simplicity, we take the $m_a \to 0$ limit so

$$q^2 = m_s^2 - 2E_s(E_s - T) + 2(E_s - T)\sqrt{E_s^2 - m_s^2}\cos\theta. \quad (11)$$

As the scattering angle can vary in the range given by Eq. (6) (unlike the above elastic scattering case where $\cos\theta$ is fixed), it is possible to find values of T for a given m_s such that the $q^2 = 0$ pole is kinematically accessible.

In order to obtain a physical, finite differential cross section, the singularity due to the real photon pole needs regularization. Notice that when the exchanged virtual photon approaches the on-shell limit $q^2 = 0$, the scattering process is no longer distinguishable from a two-step process in which the sterile neutrino first undergoes a radiative decay and the emitted real photon subsequently causes the atomic ionization. This two-step process causes an attenuation of the real photon intensity in dense detector media, and can be easily implemented by adding a small imaginary part to the wave number, i.e.,

$$|\vec{q}| \to |\vec{q}| + \frac{i}{2} n_{\mathrm{A}} \sigma_\gamma(\mathrm{A}, |\vec{q}|), \quad (12)$$

where n_{A} is the number density of scatterers A in the detector and $\sigma_\gamma(\mathrm{A}, |\vec{q}|)$ is the photoabsorption cross section of one single scatterer A with photon energy $T = |\vec{q}|$. As a result,

$$|\vec{q}|^2 \to |\vec{q}|^2 - \frac{1}{4}n_{\mathrm{A}}^2\sigma_\gamma^2 + i|\vec{q}|n_{\mathrm{A}}\sigma_\gamma(\mathrm{A}, |\vec{q}|) \approx |\vec{q}|^2 + i|\vec{q}|n_{\mathrm{A}}\sigma_\gamma(\mathrm{A}, |\vec{q}|), \quad (13)$$

and the photon propagator is regularized by

$$\frac{1}{q^2} \to \frac{1}{q^2 - i|\vec{q}|n_{\rm A}\sigma_\gamma({\rm A}, |\vec{q}|)}.$$

Using this ansatz, the regularized differential cross section (denoted by a bar)

$$\frac{d\bar{\sigma}}{dT} = \int d\cos\theta \frac{2\pi\alpha^2}{(q^2)^2 + (|\vec{q}|n_{\rm A}\sigma_\gamma({\rm A}, |\vec{q}|))^2} \frac{|\vec{k}_a|}{|\vec{k}_s|} \times \left(\frac{\mu_{\nu_{\rm sa}}}{2m_e}\right)^2 (V_L R_L + V_T R_T) \quad (14)$$

is free of singularity, and away from the pole region $q^2 \to 0$, the regulator $|\vec{q}|n_{\rm A}\sigma_\gamma({\rm A}, |\vec{q}|)$ has a negligible impact.

A. Some approximation schemes

Full calculations of $d\bar{\sigma}/dT$ require many-body wave functions so that the response functions R_L and R_T can be evaluated. In most cases, these are highly nontrivial. We discuss in the following a few approximation schemes that help to simplify the many-body problems in certain, if not all, kinematic regions.

First, when the real photon pole $q^2 \to 0$ is accessed (or approached) in a scattering process, it is natural to expect that the equivalent photon approximation (EPA),

$$\left.\frac{d\bar{\sigma}}{dT}\right|_{\rm EPA} = \left(\frac{\mu_{\nu_{\rm sa}}}{2m_e}\right)^2 \frac{\alpha}{\pi} \frac{|\vec{k}_a|}{|\vec{k}_s|} T\sigma_\gamma({\rm A}, T) \times \int d\cos\theta \frac{V_T}{q^4 + (|\vec{q}|n_{\rm A}\sigma_\gamma({\rm A}, |\vec{q}|))^2}, \quad (15)$$

should work, as the pole region dominates the differential cross section. In our case, it can be easily worked out that for energy transfer T within the interval $[(E_s - |\vec{k}_s|)/2, (E_s + |\vec{k}_s|)/2]$, a photon pole always occurs at some certain scattering angle.[2]

Under further approximations that (i) $V_T \approx (m_s^2 - m_a^2)^2$, which is the most singular term in V_T that comes with a double pole $1/(q^2)^2$, and (ii) the regulator can be set to a constant $Tn_{\rm A}\sigma_\gamma({\rm A}, T)$ since it is only important when $|\vec{q}| = T$, the integration of the EPA formula can be simplified and yields

$$\left.\frac{d\bar{\sigma}}{dT}\right|^{\rm pole}_{\rm EPA} \approx \left(\frac{\mu_{\nu_{\rm sa}}}{2m_e}\right)^2 \frac{\alpha}{2\pi} \frac{1}{|\vec{k}_s|^2} \frac{(m_s^2 - m_a^2)^2}{n_{\rm A}} \times \tan^{-1}\left(\frac{q^2}{Tn_{\rm A}\sigma_\gamma({\rm A}, T)}\right)\Bigg|^{q^2_{\rm max}}_{q^2_{\rm min}}, \quad (16)$$

$$\approx \left(\frac{\mu_{\nu_{\rm sa}}}{2m_e}\right)^2 \frac{\alpha}{2n_{\rm A}} \frac{(m_s^2 - m_a^2)^2}{|\vec{k}_s|^2}, \quad \text{if } |q^2_{\rm max}| \text{ and } |q^2_{\rm min}| \gg Tn_{\rm A}\sigma_\gamma({\rm A}, T). \quad (17)$$

The last line shows that for cases where both $|q^2_{\rm max}|$ and $|q^2_{\rm min}|$ are much larger than the regulator $Tn_{\rm A}\sigma_\gamma({\rm A}, T)$, the approximated EPA result takes an extremely simple form that is independent of T, as long as $(E_s - |\vec{k}_s|)/2 \le T \le (E_s + |\vec{k}_s|)/2$. In later sections, we will give examples for such a plateaulike pattern in $d\bar{\sigma}/dT$ to illustrate this point.

Second, in contrast to the EPA, one can keep only the longitudinal response R_L by setting $V_T = 0$ in Eq. (14). This corresponds to the case where the exchanged photon is purely longitudinal, so it is called the longitudinal photon approximation (LPA). Depending on the kinematics of the processes being considered, the LPA can work well, in particular for the cases where the atomic 3-current density is relatively suppressed compared with the charge density in a nonrelativistic expansion, or the exchanged photon is not close to real since there is no $q^2 = 0$ pole in V_L/q^4.

Last but not least, one can neglect the binding effect on atomic wave functions and treat atomic electrons as free particles, as long as the deposited energy T is big enough to yield ionization. This free electron approximation (FEA) is done by multiplying the scattering cross section of free electrons, $d\bar{\sigma}^{(\nu e)}/dT$, by the number of bound electrons that can be ionized with a given T:

$$\left.\frac{d\bar{\sigma}}{dT}\right|_{\rm FEA} = \sum_i \theta(T - B_i) \frac{d\bar{\sigma}^{(\nu_s e \to \nu_a e)}}{dT}, \quad (18)$$

where

$$\frac{d\bar{\sigma}^{(\nu_s e \to \nu_a e)}}{dT} = \left(\frac{\mu_{\nu_{\rm sa}}}{2m_e}\right)^2 \frac{\pi\alpha^2}{m_e|\vec{k}_s|^2} \frac{1}{q^4 + (|\vec{q}|n_{\rm A}\sigma_\gamma({\rm A}, |\vec{q}|))^2} \times \{(q^2(m_s + m_a)^2 - (m_s^2 - m_a^2)^2)(2m_e^2 + q^2) - q^4(m_s^2 + m_a^2) - 2q^2 m_e(2E_s - T)(m_1^2 - m_2^2) - 8q^2 m_e^2 E_s(E_s - T)\}|_{q^2 = -2m_e T}. \quad (19)$$

Note that $q^2 = -2m_e T < 0$ in the FEA, so the real photon pole cannot be reached, and the regulator has negligible impact.

III. HYDROGEN CASE

In this section, we consider the hydrogen atom as the target with different combinations of sterile neutrino masses m_s and velocities v_s. The number density of hydrogen atoms is taken to be the one in water, i.e., $n_{\rm H} = 6.6 \times 10^{22}/{\rm cm}^3$, and this gives the regulator $|\vec{q}|n_{\rm H}\sigma_\gamma({\rm H}, |\vec{q}|) \lesssim 120\ {\rm eV}^2$ in the allowed range of $|\vec{q}|$ (the regulator decreases with increasing $|\vec{q}|$). Note that most calculations with hydrogen can be done analytically by standard techniques, and details be found in Ref. [26].

[2]Note that the physical range of T is between $[B, E_s]$.

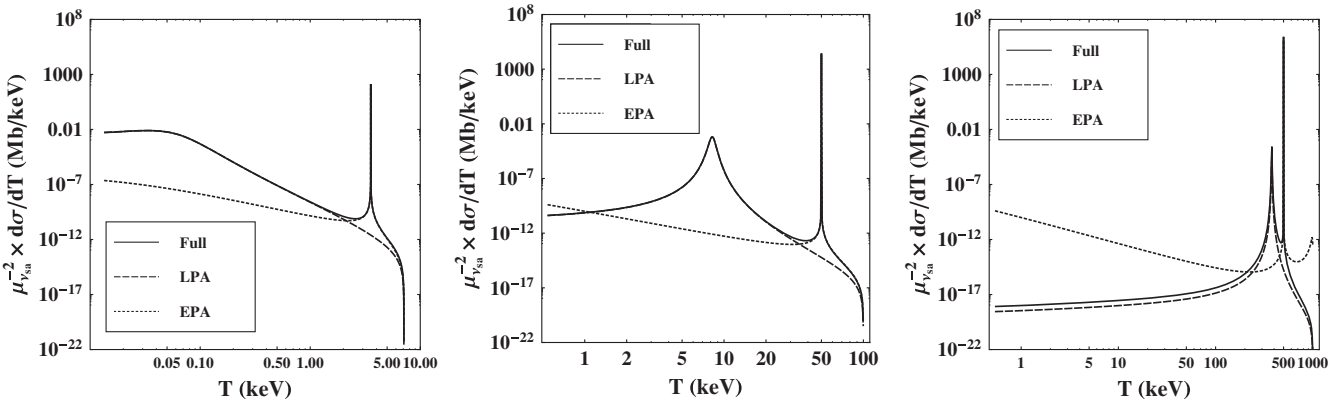

(a) $m_s = 7.1\,\mathrm{keV}$ (b) $m_s = 100\,\mathrm{keV}$ (c) $m_s = 1\,\mathrm{MeV}$

FIG. 2. The differential scattering cross sections of nonrelativistic sterile neutrinos ($v_s = 10^{-3}$) and hydrogen atoms through the transition magnetic moment $\mu_{\nu_{sa}}$ with selected m_s.

A. $m_s = 7.1$ keV, $v_s = 10^{-3}$

Suppose the x-ray anomaly hints the existence of 7.1-keV-mass sterile neutrinos as a form of cold dark matter (DM) in our galaxy with NR velocity on the order of 10^{-3}. Their differential scattering cross section on hydrogen atoms through the transition magnetic moment $\mu_{\nu_{sa}}$ is shown in Fig. 2(a). As can be seen from the plot, there is a pronounced peak at $T \sim m_s/2 = 3.55$ keV. This is due to the real photon kinematics being accessed, which also explains why the EPA works well around the near-pole region. Away from this peak region, because there is no more strong $1/q^4$ enhancement ($q^2 \to 0$ cannot be reached) that can overcome the nonrelativistic suppression of the transverse current density over the charge density (order v/c vs order 1), the LPA becomes a better approximation instead.

B. $m_s = 100$ keV; 1 MeV, $v_s = 10^{-3}$

Consider the mass of the NR sterile neutrino is increased to 100 keV and 1 MeV, the differential cross sections are shown in Figs. 2(b) and 2(c), respectively. Unlike the previous case with $m_s = 7.1$ keV, $d\sigma/dT$ now exhibits a twin-peak pattern. The peak at $T = m_s/2 = 50$ keV or 500 keV is the one that is due to the double pole in the photon propagator (so well approximated by the EPA). Compared with the peak in the $m_s = 7.1$ keV case, not only its absolute value increases as m_s^2 [see Eq. (17)], but also it stands out more significantly from the rest nonpeak region, where the atomic longitudinal response is more suppressed because of a bigger momentum transfer that gives rise to a more oscillating function to be integrated.

The other peak at $T \sim 8.18$ keV or 333 keV, which falls in the region where the LPA is good, can be understood as follows: The maximum of the longitudinal response, Eq. (7), is reached under the condition: $|\vec{q}| \sim |\vec{p}_r| \approx |\vec{p}_e|$; in other words, the momentum (and energy, too) transfer is purely taken by the electron, while the proton is just a spectator. In this case, the scattering appears to be a two-body process so that $q^2 \approx -2m_e T$ and $\vec{q}^2 \approx (m_s - T)^2$. As a result, the energy transfer that gives rise to this peak due to two-body kinematics is

$$T^{(\nu e)} = \frac{m_s^2}{2(m_s + m_e)}. \tag{20}$$

For $m_s = 7.1$ keV, one would predict a similar peak happening at $T^{(\nu e)} = 48.6$ keV; in fact this can be readily seen in Fig. 2(a) but without a sharp contrast, for kinematic reason just discussed.

C. $m_s = 7.1$ keV, $v_s \to 1$

As there might be possible mechanisms to boost cold DM candidates, it is also interesting to consider relativistic 7.1-keV-mass sterile neutrinos. For this case, we need to discuss first the broadening effect in decay and scattering of boosted sterile neutrinos.

Suppose the sterile neutrino moves with some relativistic velocity $v_s \to 1$. In the rest frame of the sterile neutrino, when it breaks up into a photon and a light neutrino (taken to be massless in our consideration), the energy of the photon has a single value $m_s/2$. After transforming back to the laboratory frame, the photon energy spectrum is broadened to a region with a width depending on v_s. This broadening effect also manifests in our considered process: As the double-pole position, which is determined by the real photon energy, can take on a finite range of value, the sharp peak in the differential cross section in the nonrelativistic case is broadened to be like a plateau.

The plots in Fig. 3 show the results for a relativistic 7.1-keV sterile neutrino with energy of (a) 10 keV, (b) 100 keV, and (c) 1 MeV, respectively. Comparing these three cases, which differ in relativistic degree, and also the exact versus

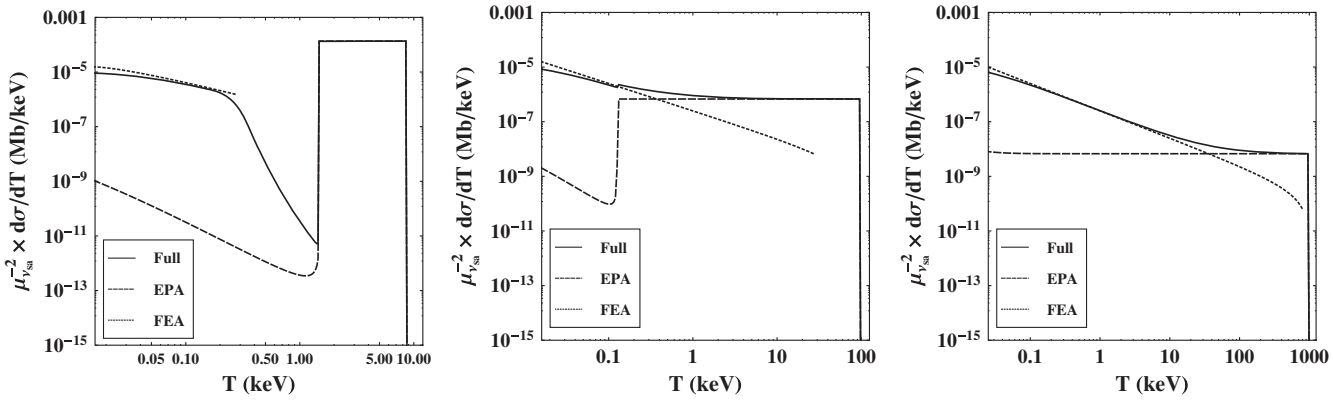

(a) $E_s = 10\,\mathrm{keV}$ (b) $E_s = 100\,\mathrm{keV}$ (c) $E_s = 1\,\mathrm{MeV}$

FIG. 3. The differential scattering cross sections of relativistic sterile neutrinos ($m_s = 7.1$ keV) and hydrogen atoms through the transition magnetic moment $\mu_{\nu_{sa}}$ with selected E_s.

approximated results, one can observe several important features.

(i) For T above certain values until the end point, i.e., E_ν, the differential cross sections all behave like T-independent plateaux, which can be well described by the EPA. This plateaulike structure is mainly due to the broadening of the double-pole peak and roughly scales as $|\vec{k}_s| \sim E_s$, as explained in the previous section. Also, because the EPA works well, the heights of these plateaux scale as $1/|\vec{k}_s|^2 \sim 1/E_\nu^2$, as anticipated by Eq. (17).

(ii) For smaller T, even when it still lies in the range where a double pole is allowed kinematically, the EPA stops to be a good approximation. This indicates that the longitudinal response starts to contribute significantly. As can be seen from the figure, the exact calculation overlaps less with the EPA plateau as the incident sterile neutrino becomes more relativistic.

(iii) In the medium to low T region, on the contrary, the FEA becomes a good approximation. In fact, with the incident sterile neutrinos becoming more relativistic, it has a wider range of applicability. For example, in the $E_s =$ 1 MeV case, the FEA works well from near threshold all the way to $T \sim 50$ keV. Since the mass of the sterile neutrino becomes negligible in the ultrarelativistic limit, the differential cross section coverages to the one of neutrino magnetic moment studies with active neutrinos. The latter case has been extensively studied in hydrogen [26] and complex atoms such as germanium [27], all results show that the FEA indeed is a good approximation for T away from the threshold and end point.

IV. GERMANIUM CASE

Low threshold germanium detectors with sub-keV sensitivities have played an important roles in neutrino and dark matter experiments [28]. In particular, they have been used to provide the stringent limits on neutrino magnetic moments [29–32] and neutrino millicharge [33]. The derivations formulated in earlier sections are now extended to the germanium atom in this section.

The number density of germanium atoms in typical semiconductor detectors is $n_{\mathrm{Ge}} = 4.42 \times 10^{22}/\mathrm{cm}^3$, and this gives the regulator $|\vec{q}| n_{\mathrm{H}} \sigma_\gamma(\mathrm{H}, |\vec{q}|) \lesssim 1200\ \mathrm{eV}^2$ in the allowed range of $|\vec{q}|$ (the regulator decreases with increasing $|\vec{q}|$). The atomic many-body physics is handled by the multiconfiguration relativistic random phase approximation (MCRRPA) (see, e.g., [34,35]). The method has been benchmarked and applied to our previous work on normal neutrino scattering through electroweak interactions, and details can be found in Ref. [36].

Figure 4(a) shows the results for the case: $m_s = 7.1$ keV and $v_s = 10^{-3}$. The peak region around $T = m_s/2 =$ 3.5 keV to the end point is well approximated by the EPA, while at low recoil energies, $T \lesssim 1$ keV, the LPA works better. In the transition region between 1 and 3 keV, the transverse and longitudinal responses contribute similarly in magnitude so neither approximations are valid. The sharp edge observed at $T \sim 1.3$ keV corresponds to the opening of $n = 2$ shells, which have ionization energies 1.26, 1.29, and 1.45 keV for $2p_{3/2}$, $2p_{1/2}$, and $2s_{1/2}$ orbitals, respectively, as calculated by MCRRPA [27,36]. There are similar edges for higher orbitals (140, 145, and 202 eV for $3p_{3/2}$, $3p_{1/2}$, and $3s_{1/2}$ orbitals, respectively), however, they are not resolved on this log-log plot.

When m_s is increased to 20 keV, with the same NR velocity, the results are plotted in Fig. 4(b). The double-pole peak is shifted to $T = m_s/2 = 10$ keV in the case, with the peak value bigger than the $m_s =$ 7.1 keV case by about 1 order of magnitude. This can be explained by the EPA formula, Eq. (17), that $d\bar{\sigma}/dT \propto m_s^2$, so $(20\ \mathrm{keV}/7.1\ \mathrm{keV})^2 = 10$. Various edges mentioned previously are now resolved better in this plot. The peak at $T \sim 370$ eV is the one corresponding to two-body ν_s–e scattering mentioned previously, with the position

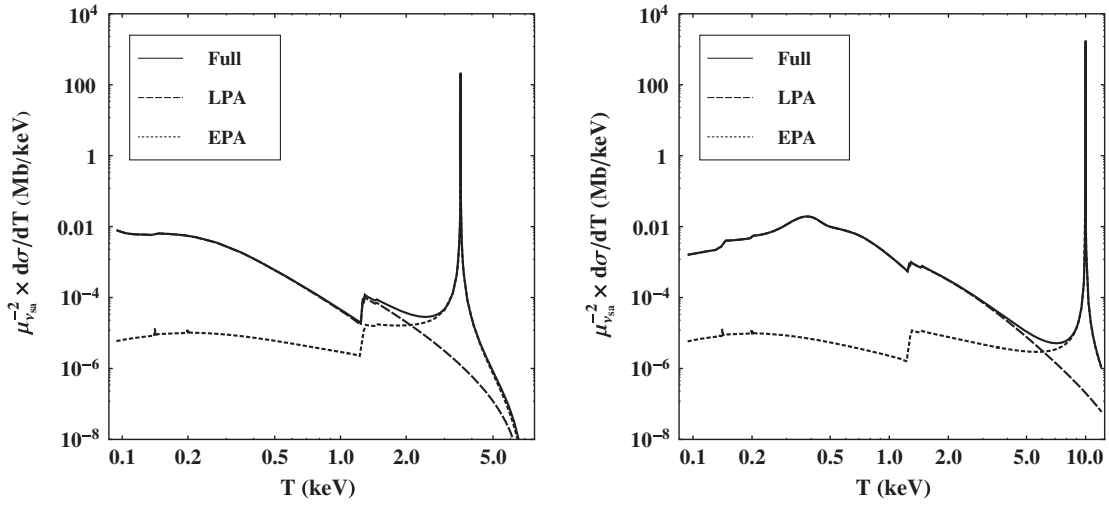

(a) $m_s = 7.1\,\mathrm{keV}$ (b) $m_s = 20\,\mathrm{keV}$

FIG. 4. The differential scattering cross section of nonrelativistic sterile neutrinos ($v_s = 10^{-3}$) and germanium atoms through the transition magnetic moment $\mu_{\nu_{sa}}$ with selected m_s.

predicted by Eq. (20). [Note that the two-body peak for the $m_s = 7.1$ keV case happens at $T \sim 50$ eV, which is outside the plot range of Fig. 4(a)].

Results for an ultrarelativistic 7.1-keV sterile neutrino of $E_s = 1$ MeV are given in Fig. 5. For T between 1 to 10 keV, the FEA agrees with the MCRRPA result; for T below 1 keV, the FEA slightly overshoots and differs from the MCRRPA result by about a factor of 2 at $T = 100$ eV. Notice that these two curves are almost identical to what have been shown in the upper panel of Fig. 2 of Ref. [27],

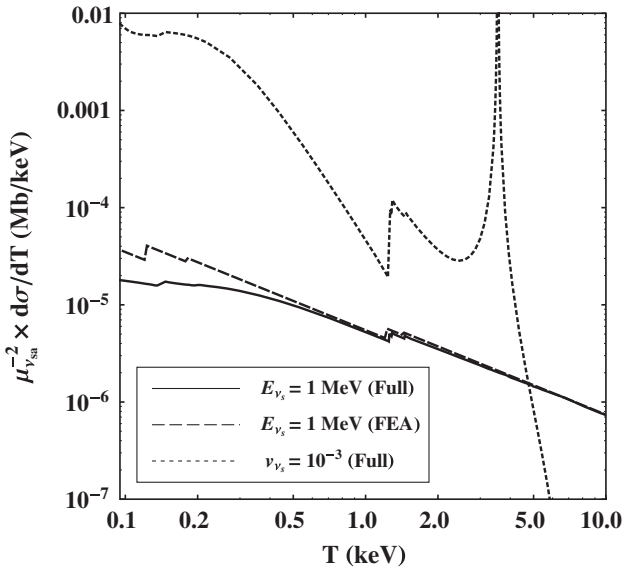

FIG. 5. The differential scattering cross section of relativistic sterile neutrinos and germanium atoms through the transition magnetic moment $\mu_{\nu_{sa}}$ with $m_s = 7.1$ keV and $E_\nu = 1$ MeV (solid line). For comparison, the results of free electron approximation (dashed line) and the nonrelativistic case with $v_s = 10^{-3}$ (dotted line) are also shown.

where neutrino magnetic moments of active neutrinos were considered. In other words, the transition magnetic moment arising from the sterile-to-active neutrino conversion is indistinguishable from those from active neutrino mixings, as we can take the zero mass limit for sterile and active neutrinos in a relativistic process. In the same figure, we also compare the ultrarelativistic and nonrelativistic 7.1-keV sterile neutrinos: In this low-recoil regime being considered, 100 eV $\leq T \leq$ 10 keV, germanium detectors are more sensitive to the nonrelativistic sterile neutrinos for they yield bigger differential cross sections in general and exhibit rich, unique structure (can be resolved by detectors with fine resolutions).

V. BOUNDS ON STERILE NEUTRINO PROPERTIES

A data sample of 139.3 kg-days with a 500 g n-type point contact germanium detector taken at the Kuo-Sheng Reactor Neutrino Laboratory (KSNL) [30,37] were analyzed. The measured spectra after standard background suppression [29,30,37] is depicted in Fig. 6(a). A dark matter analysis searching for the atomic ionization interaction of Eq. (21) is applied to the data, using conventional astrophysical models on the sterile neutrino as cold dark matter.

The local dark matter density of $\rho = 0.4$ GeV cm^{-3} is adopted [38]. The event rate per unit mass on a target of germanium is given by

$$\left(\frac{dR}{dT}\right) = \frac{\rho_s}{m_{\mathrm{A}} m_s} \int_0^{v_{\max}} \frac{d\sigma(m_s, v)}{dT} v f(\vec{v}) d^3 v, \quad (21)$$

where m_{A} is the mass of the germanium atom and m_s denotes the mass of sterile neutrino. The normalized Maxwellian velocity distribution

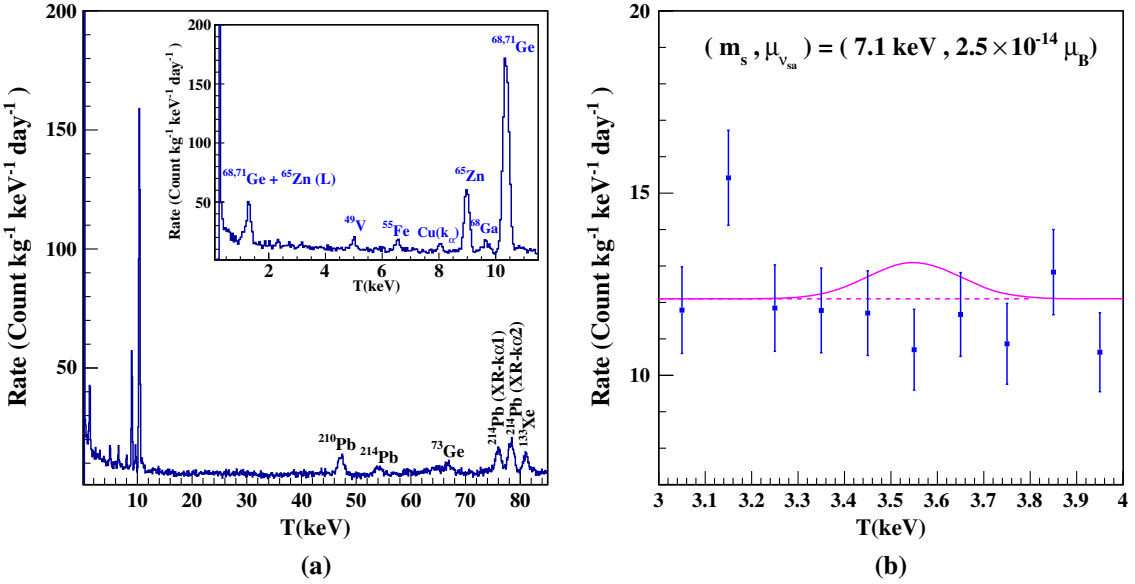

FIG. 6. Experimental data and analysis: (a) Measured spectrum of germanium detector at KSNL. All peaks can be accounted for by internal and ambient radioactivity. (b) The zoomed energy range relevant to a ν_s with $m_s = 7.1$ keV. The spectrum due to $\mu_{\nu_{sa}} = 2.5 \times 10^{-14}\mu_B$ excluded at 90% C.L. is superimposed.

$$f(\vec{v}) = N_0 e^{(-\vec{v}^2/v_0^2)}\Theta(v_{esc} - |\vec{v}|), \tag{22}$$

where N_0 is the normalization value and Θ denotes the Heaviside step function. The dark matter particle has a mean velocity $v_0 = 220$ km/s and escape velocity $v_{esc} = 533$ km/s in Earth's reference frame [39].

Sterile neutrinos would manifest themselves experimentally as an excess of events over understood background with a peak-shaped spectrum like that of Fig. 6(b), obtained by smearing the theoretical signal of Fig. 4(a) with the detector resolution. The data are analyzed by using the simplified differential cross-section formula Eq. (17), as the EPA provides a good approximation in this region. A minimal χ^2 analysis is applied with two free parameters describing a locally smooth background and $\mu_{\nu_{sa}}$. As an illustration, the measurement for the case $m_s = 7.1$ keV is displayed in Fig. 6(b) and the excluded spectrum at 90% C.L. is superimposed.

The exclusion plot of transition magnetic moment ($\mu_{\nu_{sa}}$) versus mass (m_s) at 90% C.L. is illustrated in Fig. 7. The bump structures in the exclusion correspond to the background peaks from known radioactivity—for instance, the drop in sensitivity at $m_s \sim 20$ keV is a consequence of increased background due to the germanium x-ray peak at 10.37 keV (K-shell). At $m_s = 7.1$ keV, the upper limit of $\mu_{\nu_{sa}} < 2.5 \times 10^{-14}\mu_B$ at 90% C.L. is derived.[3] In comparison, the laboratory upper limits of the magnetic moments of ν_e and $\nu_{\bar{e}}$ are $1.3 \times 10^{-8}\mu_B$ [40] and $2.9 \times 10^{-11}\mu_B$ [32], respectively. The reason for a better sensitivity in our current case is mainly due to the enhancement in the differential cross section. We also note that the sterile neutrino DM flux on Earth at $m_s = 7.1$ keV is of the same order of magnitude as the reactor electron antineutrino flux at KSNL at a distance of 28 m from the reactor core.

The radiative decay lifetime and transition magnetic moment of a sterile neutrino can be related by Eq. (2), so

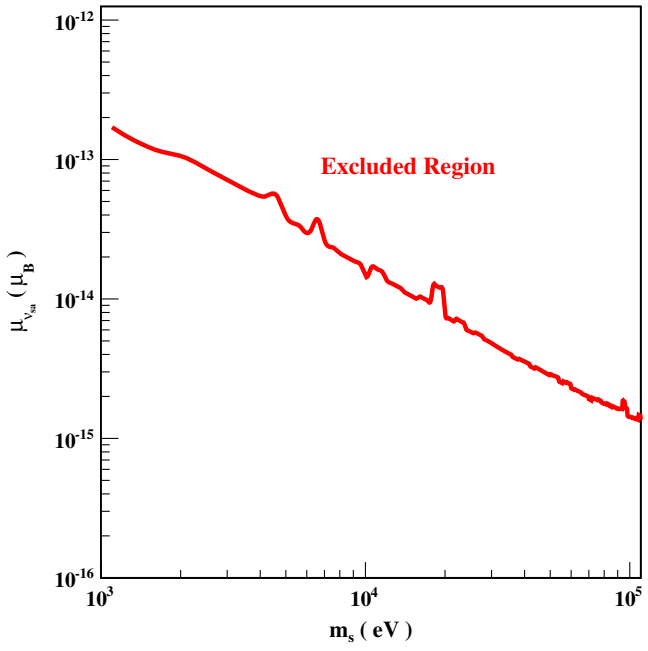

FIG. 7. Exclusion curve at 90% C.L. for the absolute value of the transition magnetic moment of sterile neutrinos, based on reactor neutrino data of Fig. 6.

[3]More precisely, it is the upper limit on the absolute value of $\mu_{\nu_{sa}}$, as the experimental rate is proportional to $\mu^2_{\nu_{sa}}$.

the recent identification of a 7.1 keV sterile neutrino with $\Gamma_{\nu_s\to\nu_a\gamma} = 1.74 \times 10^{-28}$ s^{-1}, based on the astrophysical x-ray observations [19,20], can be converted to $\mu_{\nu_{sa}} = 2.9 \times 10^{-21}\mu_B$. This astrophysical determination exceeds our direct detection bounds by several orders of magnitude, mainly because its much larger collecting volume.

VI. SUMMARY

The transition magnetic moment of a sterile-to-active neutrino conversion gives rise to not only radiative decay of a sterile neutrino, but also its nonstandard interaction (NSI) with matter. In this paper, we consider the atomic ionization due to such a NSI, including hydrogen and germanium. This is a doubly inelastic scattering with both the projectile and the target changing their internal states—massive to massless neutrino in the former and an atom to an ion plus a free electron in the latter. Accordingly, the kinematics can have a crossover between the spacelike and timelike regions in a certain range of energy transfer T, such that the differential cross section is enhanced whenever the exchanged photon approaches the real photon limit. For a nonrelativistic sterile neutrino with mass m_s and velocity $v_s \ll 1$, it is found that the differential cross section exhibits a peak that centers at $T \approx m_s/2$ with the width $\propto v_s$ and maximum value $\propto m_s^2/v_s^2$. When the sterile neutrino becomes more relativistic, the peak is smeared out due to the relativistic broadening, so the transition magnetic moment of a sterile neutrino is then indistinguishable from the ones of active neutrinos.

Using the data taken by the TEXONO germanium detectors, which have fine energy resolution in keV and sub-keV regimes, we derive constraints on the mass and transition magnetic moment $\mu_{\nu_{sa}}$ of a sterile neutrino as the dark matter particle. For m_s in the range of a few keV to 100 keV, the upper limit on $\mu_{\nu_{sa}}$ drops from $\sim 10^{-13}\mu_B$ to $\sim 10^{-15}\mu_B$ with increasing m_s. These constraints are better than the current direct limits on the magnetic moments of active neutrinos, $\sim 10^{-11}\mu_B$, mainly because of the much enhanced scattering cross sections at $T \approx m_s/2$. On the other hand, the astrophysical hints of a 7.1-keV sterile neutrino with radiative decay rate $\Gamma_{\nu_s\to\nu_a\gamma} = 1.74 \times 10^{-28}$ s^{-1} would imply a more sensitive determination of $\mu_{\nu_{sa}} = 2.9 \times 10^{-21}\mu_B$, due to the huge collecting volume of galactic scales.

ACKNOWLEDGMENTS

We acknowledge the support from the Ministry of Science and Technology, Taiwan, under Grants No. 102-2112-M-002-013-MY3 (J.-W. C., C.-L. W., and C.-P. W.), No. 103-2112-M-259-003 and No. 104-2112-M-259-004-MY3 (C.-P. L.), No. 104-2112-M-001-038-MY3 (H. T. W. and L. S.); the Center for Theoretical Sciences and Center of Advanced Study in Theoretical Sciences of National Taiwan University (J.-W. C., C.-L. W., and C.-P. W.); and the National Center for Theoretical Sciences. J.-W. C. would like to thank the hospitality of the Rudolph Peierls Centre for Theoretical Physics of the University of Oxford and Oxford Holography group, DAMTP of University of Cambridge, and Helmholtz-Institut für Strahlen-und Kernphysik and Bethe Center for Theoretical Physics, Universität Bonn.

[1] P. Minkowski, Phys. Lett. B **67**, 421 (1977).
[2] P. Ramond, in International Symposium on Fundamentals of Quantum Theory and Quantum Field Theory, Palm Coast, Florida, 1979, pp. 265–280 [arXiv:hep-ph/9809459].
[3] R. N. Mohapatra and G. Senjanovic, Phys. Rev. Lett. **44**, 912 (1980).
[4] T. Yanagida, Prog. Theor. Phys. **64**, 1103 (1980).
[5] J. Schechter and J. W. F. Valle, Phys. Rev. D **22**, 2227 (1980).
[6] K. Abazajian, M. Acero, S. Agarwalla, A. Aguilar-Arevalo, C. Albright *et al.*, arXiv:1204.5379.
[7] A. de Gouvea, Phys. Rev. D **72**, 033005 (2005).
[8] J. Kopp, M. Maltoni, and T. Schwetz, Phys. Rev. Lett. **107**, 091801 (2011).
[9] A. Aguilar-Arevalo *et al.* (LSND Collaboration), Phys. Rev. D **64**, 112007 (2001).
[10] G. Mention, M. Fechner, T. Lasserre, T. A. Mueller, D. Lhuillier, M. Cribier, and A. Letourneau, Phys. Rev. D **83**, 073006 (2011).
[11] T. Asaka, S. Blanchet, and M. Shaposhnikov, Phys. Lett. B **631**, 151 (2005).
[12] T. Asaka and M. Shaposhnikov, Phys. Lett. B **620**, 17 (2005).
[13] S. Dodelson and L. M. Widrow, Phys. Rev. Lett. **72**, 17 (1994).
[14] X.-D. Shi and G. M. Fuller, Phys. Rev. Lett. **82**, 2832 (1999).
[15] A. D. Dolgov and S. H. Hansen, Astropart. Phys. **16**, 339 (2002).
[16] K. Abazajian, G. M. Fuller, and M. Patel, Phys. Rev. D **64**, 023501 (2001).
[17] K. Abazajian, G. M. Fuller, and W. H. Tucker, Astrophys. J. **562**, 593 (2001).

[18] A. Boyarsky, A. Neronov, O. Ruchayskiy, M. Shaposhnikov, and I. Tkachev, Phys. Rev. Lett. **97**, 261302 (2006).
[19] E. Bulbul, M. Markevitch, A. Foster, R. K. Smith, M. Loewenstein and S. W. Randall, Astrophys. J. **789**, 13 (2014).
[20] A. Boyarsky, O. Ruchayskiy, D. Iakubovskyi, and J. Franse, Phys. Rev. Lett. **113**, 251301 (2014).
[21] V. B. Semikoz and J. W. F. Valle, Nucl. Phys. **B425**, 651 (1994); **B485**, 545(E) (1997).
[22] S. Sahu and V. M. Bannur, Phys. Rev. D **61**, 023003 (1999).
[23] S. N. Gninenko and N. V. Krasnikov, Phys. Lett. B **450**, 165 (1999).
[24] A. B. Balantekin and N. Vassh, Phys. Rev. D **89**, 073013 (2014).
[25] P. B. Pal and L. Wolfenstein, Phys. Rev. D **25**, 766 (1982).
[26] J.-W. Chen, C.-P. Liu, C.-F. Liu, and C.-L. Wu, Phys. Rev. D **88**, 033006 (2013).
[27] J.-W. Chen, H.-C. Chi, K.-N. Huang, C.-P. Liu, H.-T. Shiao, L. Singh, H. T. Wong, C.-L. Wu, and C.-P. Wu, Phys. Lett. B **731**, 159 (2014).
[28] A. K. Soma *et al.* (TEXONO Collaboration), arXiv: 1411.4802.
[29] H. Li *et al.* (TEXONO Collaboration), Phys. Rev. Lett. **90**, 131802 (2003).
[30] H. T. Wong *et al.* (TEXONO Collaboration), Phys. Rev. D **75**, 012001 (2007).
[31] A. G. Beda, V. B. Brudanin, V. G. Egorov, D. V. Medvedev, V. S. Pogosov, M. V. Shirchenko, and A. S. Starostin, Adv. High Energy Phys. **2012**, 350150 (2012).
[32] A. Beda, V. Brudanin, V. Egorov, D. Medvedev, V. Pogosov E. A. Shevchik, M. V. Shirchenko, A. S. Starostin, and I. V. Zhitnikov, Phys. Part. Nucl. Lett. **10**, 139 (2013).
[33] J.-W. Chen, H.-C. Chi, H.-B. Li, C. P. Liu, L. Singh, H. T. Wong, C.-L. Wu, and C.-P. Wu, Phys. Rev. D **90**, 011301 (2014).
[34] K.-N. Huang and W. R. Johnson, Phys. Rev. A **25**, 634 (1982).
[35] K.-N. Huang, H.-C. Chi, and H.-S. Chou, Chin. J. Phys. **33**, 565 (1995).
[36] J.-W. Chen, H.-C. Chi, K.-N. Huang, H.-B. Li, C.-P. Liu, L. Singh, H. T. Wong, C.-L. Wu, and C.-P. Wu, Phys. Rev. D **91**, 013005 (2015).
[37] M. Deniz *et al.* (TEXONO Collaboration), Phys. Rev. D **81**, 072001 (2010).
[38] R. Catena and P. Ullio, J. Cosmol. Astropart. Phys. 08 (2010) 004.
[39] T. Piffl *et al.*, Astron. Astrophys. **562**, A91 (2014).
[40] B. Xin *et al.* (TEXONO Collaboration), Phys. Rev. D **72**, 012006 (2005).